Chinese Chemical Letters 33 (2022) 415–423

Contents lists available at ScienceDirect

Chinese Chemical Letters

journal homepage: www.elsevier.com/locate/cclet

Communication

Effective *E. coli* inactivation of core-shell ZnO@ZIF-8 photocatalysis under visible light synergize with peroxymonosulfate: Efficiency and mechanism

Yanni Jiang[a,b], Zhaokun Xiong[a,b], Jianbo Huang[c], Feng Yan[c,*], Gang Yao[b,d], Bo Lai[a,b,**]

[a] State Key Laboratory of Hydraulics and Mountain River Engineering, College of Architecture and Environment, Sichuan University, Chengdu 610065, China
[b] Sino-German Centre for Water and Health Research, Sichuan University, Chengdu 610065, China
[c] Department of Ultrasound, Laboratory of Ultrasound Imaging Drug, West China Hospital, Sichuan University, Chengdu 610041, China
[d] Institute of Environmental Engineering, RWTH Aachen University, Aachen 52072, Germany

ARTICLE INFO

Article history:
Received 18 March 2021
Revised 21 April 2021
Accepted 23 June 2021
Available online 1 July 2021

Keywords:
Bacterial inactivation
Photocatalysis
Visible light
Peroxymonosulfate

ABSTRACT

How to utilize inexhaustible solar light as a means of disinfection technology for its cheap and green remains a challenge. In this work, core-shell ZnO@ZIF-8 was synthesized and used for bacterial inactivation synergizing with peroxymonosulfate (PMS) under visible light irradiation. It took 50 min to achieve thorough sterilization for 7.5-log *Escherichia coli (E. coli)* cells in vis/PMS/ZnO@ZIF-8 system, compared with that 4.5-log reduction completed in vis/PMS/ZnO system under the same conditions. The enhanced photocatalytic disinfection mechanisms of fabricated ZnO@ZIF-8 were investigated by UV–vis diffuse reflectance spectra, electrochemical impedance spectra and Mott-Schottky plots. The promoted bactericidal efficiency was attributed to higher charge-separation efficiency and stronger oxidation ability of photo-generated holes. Moreover, it was found that $^1O_2$ and $^{\cdot}OH$ induced bacterial cell lesion process, and the former was the main active species. The external reactive oxygen species (ROS) caused a series of cell wall damage, intercellular ROS up-regulation and genome DNA unwinding, finally resulted in irreversible bacterial death. A two-route mechanism in vis/PMS/ZnO@ZIF-8 system was proposed, in which the generation of $^1O_2$ was supposed as the product of the oxygen oxidation of photo-generated holes and PMS dissociation. Our work is expected to provide advanced information about a low-cost water disinfection technology of visible light photocatalysis.

With the growing number of global population and instability of climatic conditions, how to guarantee drinking water safe and accessible from contaminants and pathogenic microorganisms is a major challenge. As mentioned in World Health Organization (WHO) environmental daily report, around 80% human disease, 33% death and 80% cancer are originated from water. Moreover, the WHO household survey shows that many people use drinking water sources at high risk of fecal contamination, especially in rural areas [1]. The unassured water containing morbific agents will result in severe diseases like cholera, malaria and gastroenteritis in human body with a high probability. Besides, the COVID-19 globally broke out in late 2019, scientists found that inadequate water and sewer services might place inhabitants in remote communities at higher risk of virus spread [2,3]. Therefore, in efforts to control waterborne diseases and health issues, it is of vital importance to find a convenient and efficient microbial pathogens disinfection method.

So far, there has been a pile of water sterilization technologies such as chlorine, chlorine dioxide, ultraviolet and ozone disinfection [4,5]. Although chlorine disinfectants can efficiently inactivate bacteria in aqueous, the formation of disinfection byproducts, which may have carcinogenic effects on human health, developed to be an emerging problem [6,7]. Ultraviolet light can directly destroy DNA and inactivate microorganisms, and no byproducts come into being in this process. However, still many bacteria bring back to life after ultraviolet treatment [8], demonstrating it is not the optimal disinfection method. Compared with these two approaches, ozone is of high sterilization efficiency and no by-

* Corresponding author.
** corresponding author at: State Key Laboratory of Hydraulics and Mountain River Engineering, College of Architecture and Environment, Sichuan University, Chengdu 610065, China.
E-mail addresses: yan_feng@scu.edu.cn (F. Yan), laibo@scu.edu.cn (B. Lai).

https://doi.org/10.1016/j.cclet.2021.06.058
1001-8417/

produced toxic pollutants, but expensive [5,9]. Therefore, finding a green and low-cost disinfection method is a matter of great urgency.

Unlike those conventional reagents, visible light generated from sunlight is nontoxic, inexpensive and endlessly renewable source of clean energy, which can be considered extremely environmentally friendly [10]. ZnO has become an alternative to TiO_2 in photocatalytic reactions for its chemical and thermal stability, low cost and opto-electronic properties. It is an n-type semiconductor with a wide bandgap energy of 3.37 eV, but its low specific surface, rapid recombination of photo-generated electrons and holes limit its application. Fortunately, the photocatalytic performance of ZnO can be altered by modifying physical properties such as crystalline structure, morphology, or intrinsic defects as previous work reported [11-13]. ZIF-8 is a zeolitic imidazole-based metal-organic framework with large cavities interconnected by narrow windows, displaying good properties in adsorption, drug delivery and catalysis process [14], and it can be utilized to modify ZnO. In recent years, advanced oxidation processes (AOPs) based on persulfate (PS) and peroxymonosulfate (PMS) have gained importance as an alternative to traditional disinfection technologies [15-17]. However, there have been few reports on photocatalysis synergize with PMS in water sterilization.

Herein, core-shell ZnO@ZIF-8 was fabricated by traditional precipitation and hydrothermal method. The physicochemical properties of synthesized sample were characterized by multiple technologies. The bactericidal efficiency towards *Escherichia coli* (*E. coli*) in the presence of PMS and ZnO@ZIF-8 was investigated in detail under visible light irradiation. Then, the photocatalytic promotion mechanism was studied by photoelectrochemical methods including electrochemical impedance spectroscopy (EIS) spectra and Mott-Schottky plots. Furthermore, the mechanisms of bacterial inactivation were systematically investigated by main reactive species, cell morphology, antioxidation enzyme activity, intercellular reactive oxygen species (ROS) and genome DNA integrity. This work may provide innovative information to develop photocatalysts synergize with a thimbleful of PMS for low-cost and efficient bacterial inactivation under solar light.

ZnO was prepared by a traditional precipitation method [18]. Briefly, 100 mL mixture of 0.03 mol/L zinc nitrate hexahydrate and 0.3 mol/L sodium stearate were kept stirring continuously at room temperature for 3 h. The precipitate was centrifugated at 8000 rpm and rinsed with deionized water for three times. Then the sample was dried at 60 °C overnight and calcined at 450 °C for 2 h to get faint yellow ZnO powder. The materials and reagents details were listed in Test S1 (Supporting information).

Core-shell ZnO@ZIF-8 microspheres were synthesized by a modified method that described by Yu *et al.* [19]. Typically, 10 mmol 2-methylimidazole was dissolved in 50 mL *N,N*-dimethylformamide (DMF) and the solution was pre-heated at 70 °C. After that, 20 mL ZnO suspension (1 mmol ZnO dispersed in 20 mL water) was dropwise added into the pre-heated solution and the mixed suspension was heated at 70 °C with gentle stirring for 5 h. The resulting white precipitate was centrifugated at 8000 rpm, rinsed with DMF and dried at 60 °C for 12 h. The characterization details of the samples were provided in Test S2 (Supporting information).

In this study, gram-negative *E. coli* was chosen as the model bacterium to evaluate disinfection ability of vis/PMS/ZnO@ZIF-8 system. Typically, *E. coli* cells were cultured in a nutrient broth medium at 37 °C with a shaking speed of 180 rpm in a constant temperature shaker (ZHICHENG, Shanghai) and harvested in the late logarithmic phase. Then bacteria were centrifuged at 8000 rpm for 3 min, the cells were washed three times and resuspended with sterilized saline (0.85% NaCl) solution. Bacterial turbidity is typically measured at 600 nm in a spectrophotometer and expressed as optical density 600 (OD_{600}) [20]. *E. coli* concentration was controlled by OD_{600} at 0.1 and practical cell density was around $10^{7.5}$ colony forming units cfu/mL according to the plate count results.

The photocatalytic inactivation tests were conducted at 25 °C using 100 mL quartz photo-reactor provided with a cooling water system to maintain temperature during reaction. The bacteria solution was irradiated by an 80 W light source, white LED lamps of visible light (400–700 nm, CEL-LAB200E7, China Education Aulight). Then a certain amount of PMS and ZnO@ZIF-8 were added into the prepared *E. coli* solution. At given time intervals, aliquots were collected from the mixture and uniformly spread on nutrient agar plates after a serial of 10-fold dilutions with sterilized saline solution. Then plates were incubated at 37 °C for 24 h and the viable number of bacterial colonies was counted. The effects of different PMS concentrations, ZnO@ZIF-8 dosages, bacterial concentrations and pH values were studied. To analyze the influence of pH, HCl (0.1 mol/L) and NaOH (0.1 mol/L) were added to adjust the initial pH value. All the experiments were conducted in triplicate. The details for bacteria analytical methods can be found in Test S3 (Supporting information).

The morphologies of ZnO microsphere and core-shell ZnO@ZIF-8 were visualized by scanning electron microscopy (SEM). Low-magnification SEM image (Fig. 1a) shows that ZnO particles exhibit spherical shape and diameter ranges from 2 μm to 4 μm. High-magnification SEM image (Fig. 1c) indicates that the flower-like ZnO microspheres were formed by a large amount of nanosheets. The SEM images of ZnO shelled with ZIF-8 at low and high magnification were shown in Figs. 1b and d, respectively. It can be clearly observed that the ZnO maintained its overall shape and become more compact and denser after the growth of ZIF-8, suggesting that the ZIF-8 growth took place at the outer surface of ZnO microspheres and the gaps between ZnO nanosheets.

Furthermore, transmission electron microscopy (TEM) was used to study detailed structure of ZnO microspheres and ZnO@ZIF-8. The TEM images (Figs. 1e and g) of ZnO core depicted the sedimentary ZnO nanosheets filling the whole spherical surface. After the growth of ZIF-8 shell, there was a uniform layer of ZIF-8 covering the surface of ZnO core as Fig. 1f and h described. Due to its nano-scale feature, some clusters of ZIF-8 can be observed on the surface. By comparison, before and after the growth, microsphere surface become smoother and more compact, explicitly demonstrating the formation of ZnO@ZIF-8 core-shell structure.

As Fig. 1i shown, the surface groups of ZnO spheres, ZIF-8 particles and core-shell ZnO@ZIF-8 were analyzed by FT-IR spectra. The wide band at 3425 cm^{-1} is assigned to stretching vibrations of intermolecular hydrogen bonds. The bands at 3134 cm^{-1} and 2929 cm^{-1} are attributed to the C–H bonds of methyl and imidazole ring, respectively [21]. The band at 1583 cm^{-1} is owing to the stretching vibrations of C=N bonds in imidazole ring. The bands at 1311 cm^{-1}, 1147 cm^{-1} and 757 cm^{-1} are ascribed to plane bending of imidazole ring. The peak at 1426 cm^{-1} corresponds to the plane stretching of imidazole ring. The band at 995 cm^{-1} is due to stretching vibrations of C–N bonds in imidazole ring [22]. And the stretching vibration of C–N bonds in imidazole ring is located at 995 cm^{-1}. The band at 425 cm^{-1} is assigned to the stretching vibration of Zn-O moiety, indicating the preservation of ZnO in the structure [23]. The FT-IR spectra demonstrate the successful growth of ZIF-8 layer on ZnO spheres combining with SEM and TEM results.

To study the crystallinity, phase characteristics and purity of ZnO spheres, ZIF-8 particles and core-shell ZnO@ZIF-8, X-ray diffraction (XRD) was conducted. It can be seen in Fig. 1j that all diffraction peaks of synthesized ZIF-8 are same as the ones of simulated ZIF-8, revealing the prepared material possesses the same crystalline structure of ZIF-8. Meanwhile, the peaks

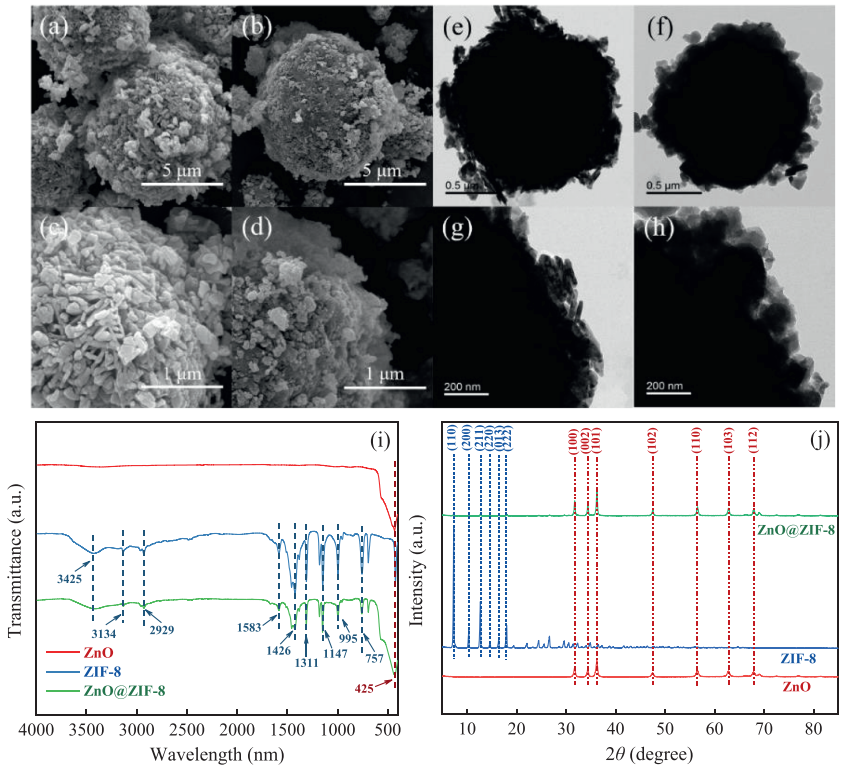

Fig. 1. SEM images of (a, c) ZnO and (b, d) ZnO@ZIF-8. TEM images of (e, g) ZnO and (f, h) ZnO@ZIF-8. (i) FT-IR and (j) XRD spectra.

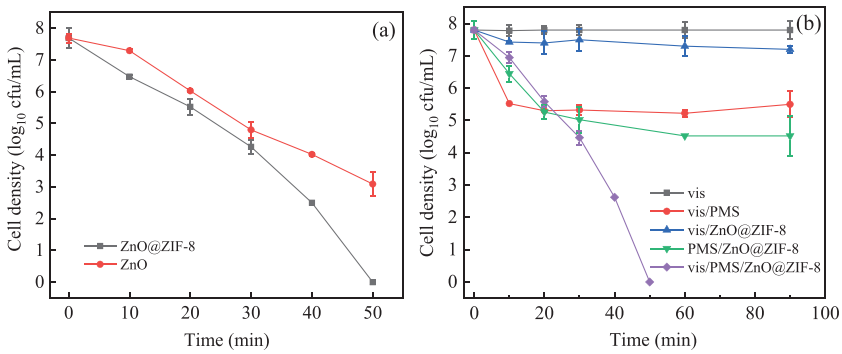

Fig. 2. (a) Bacterial inactivation efficiency in vis/PMS/ZnO and vis/PMS/ZnO@ZIF-8 systems. (b) Bacterial inactivation efficiency in vis/PMS/ZnO@ZIF-8 system and control systems including vis, vis/PMS, vis/ZnO@ZIF-8 and PMS/ZnO@ZIF-8. Experimental conditions: $T = 25$ °C; [Catalyst] = 100 mg/L; [PMS] = 0.05 mmol/L; $pH_0 = 6.5$; $\lambda \geq 400$ nm.

from ZnO spheres totally match with the typical XRD spectra of hexagonal wurtzite structure (JCPDS No. 36–1451). With these known peaks, it can be easily to identify all the peaks from ZnO@ZIF-8, which confirms the formation of ZnO@ZIF-8 core-shell structures. The typical peaks of ZIF-8 are weak in ZnO@ZIF-8 owing to its limited content and low crystallinity. XRD consequences are consistent with SEM, TEM and FT-IR observations. No other peak investigated exhibits the purity of core-shell ZnO@ZIF-8.

E. coli was chosen as the model pathogen in drinking water to evaluate the disinfection efficiency of as-prepared ZnO@ZIF-8. The bacteria inactivation behavior of vis ($\lambda \geq 400$ nm), vis/PMS, vis/ZnO@ZIF-8, PMS/ ZnO@ZIF-8, vis/PMS/ZnO and vis/PMS/ZnO@ZIF-8 was investigated. At the beginning, the sterilization efficiency variances between ZnO and core-shell ZnO@ZIF-8 were explored. In vis/PMS/ZnO@ZIF-8 system, it took 50 min to inactivate 7.5-log *E. coli* and disinfection rate reached 99.99%, which was 40% higher than vis/PMS/ZnO system (Fig. 2a). The reason might lie in the modified core-shell ZnO@ZIF-8 structure or plentiful activate sites provided by ZIF-8. As Fig. 2b shows, visible light almost has no effect on bacteria biological activity. The vis/ZnO@ZIF-8 system reduced only 0.6-log *E. coli* after 90 min, indicating ZnO@ZIF-8 showed moderate responsivity to visible light and finite activate species were produced. As a control, cytotoxicity of ZnO@ZIF-8 was studied in darkness, the results suggested that ZnO@ZIF-8 was innocuous (Fig. S1 in Supporting information). PMS, which can be activated by light, heat and transition metal ions to generate free radicals, is a kind of strong oxidant and is widely used in disinfection [24]. Karbasi *et al.* found that the addition of 10 mg/L PMS could bring a 5-fold increase on *E. coli* inactivation under visible light in their vis/PMS/3-D reduced graphene oxide system [25]. In the case of vis/PMS, it was found that around 2.3-log *E. coli* cells were inactivated in 10 min. The limited inactivation efficiency may attribute to the low concentration of PMS. Interestingly, inactivation of 3.3-log viable cells was reached in PMS/ZnO@ZIF-8 system, demonstrating there might be a synergy effect between PMS and ZnO@ZIF-8. Notably, the inactivation efficiency remarkably improved in vis/PMS/ZnO@ZIF-8 system, which is 58% higher than in PMS/ZnO@ZIF-8 system. It ac-

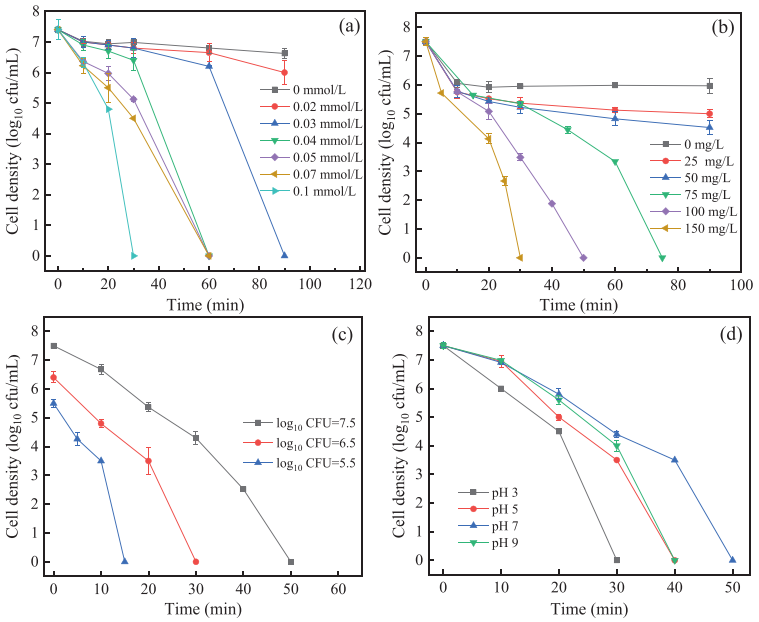

Fig. 3. Effect of experimental conditions on bacterial inactivation efficiency in vis/PMS/ZnO@ZIF-8 system: (a) PMS concentration, (b) catalyst dosage, (c) initial concentration of *E. coli*, (d) initial pH.

complished thorough disinfection in 50 min, exhibiting the best sterilization performance.

Further, PMS concentration, ZnO@ZIF-8 dosage, *E. coli* concentration and initial pH were investigated in vis/PMS/ZnO@ZIF-8 system. As shown in Fig. 3a, an increase of PMS concentration directly leaded to higher bacteria inactivation efficiency owing to the growing activate species in solution. When PMS concentration reached 0.1 mmol/L, it only took 30 min to achieve entire inactivation, which is three times faster than 0.03 mmol/L. The bactericidal performance of 0.1 mmol/L PMS as a control group was discussed in Fig. S2 (Supporting information), which indicated that it spent 60 min to complete thorough disinfection. Similarly, the bacteria inactivation efficiency has a positive correlation with the catalyst dosage (Fig. 3b). The higher dosage of ZnO@ZIF-8 attained the quicker sterilization. Increasing catalyst dosage can raise activate sites and then induced more activate species. Moreover, when the cell concentration decreased to $10^{6.5}$ and $10^{5.5}$ cfu/mL, the full inactivation was achieved within 30 min and 15 min, respectively (Fig. 3c). In addition, the effect of pH on disinfection was studied. The control experiments showed that pH ranging from 3 to 9 could not result in bacteria inactivation (Fig. S3 in Supporting information). In other words, the faint variation of bacteria biological activation caused by pH alone could be ignored. It is known that even a weakly basic environment can activate PMS to generate reactive oxygen species such as singlet oxygen, hydroxyl radical and superoxide anion [26]. As Fig. 3d presents, the inactivation efficiency obviously improved in basic pH conditions, 10 min quicker than in a neutral environment. Interestingly, when the initial pH of solution decreased to acidic condition, the bacteria inactivation efficiency was also enhanced and even behaved better than in basic solution. When pH decreased to 3, it only took 30 min to accomplish thorough disinfection. This may because the surface of *E. coli* is full of various proteins causing the cell wall to be negatively charged. In acidic conditions, protons neutralized the negative charge on the bacteria surface, reducing electrostatic repulsion between the cells and HSO_5^-, thus improving bacterial inactivation efficiency of the reaction system [27].

Fig. 4a illustrates the UV–vis diffuse reflection spectra and Tauc curves of ZnO and ZnO@ZIF-8. The UV–vis DRS results demonstrated that ZnO@ZIF-8 has a slightly better performance of light diffuse reflection than ZnO, which means the ZIF-8 shell improves the light utilization rate of ZnO. Then the optical bandgap was estimated by Tauc curves, the ZIF-8 shell reduced the band gap of ZnO particle from 3.1 eV to 2.94 eV, exhibiting a wider utilization of visible light.

In photocatalytic reactions, the migration and interface reaction ability of charges in catalysts can be studied by electrochemical impedance spectra Nyquist plots. Generally, a smaller arc radius implies smaller transfer resistance [28]. As shown in Fig. 4b, ZnO@ZIF-8 has a smaller arc radius than ZnO, indicating a higher charge-separation efficiency in the photocatalysis process, which means better photocatalytic performance.

Moreover, to study the electronic properties of ZnO microsphere and core-shell ZnO@ZIF-8, Mott-Schottky plots were carried out to study the relation between applied potential and capacitance of space charge region (Fig. 4c). Reversed sigmoidal plots were observed with an overall shape that was consistent with that of typical n-type semiconductors [29]. The intersection points of the potential and linear potential curves gave a flat band potential, which was approximately −0.906 V and −0.257 V for ZnO and ZnO@ZIF-8, respectively. Compared with the ZnO, the core-shell ZnO@ZIF-8 exhibited a positive shift on flat potential.

Since the conduction band position of n-type semiconductors is close to the flat potential, the valence band position can be reckoned by flat potential and energy band [30]. Based on the above results of Tauc curves and Mott-Schottky plots, energy band structures of ZnO and ZnO@ZIF-8 were proposed in Fig. 4d. As described in the schematic, the photoelectrons in the conduction band of ZnO@ZIF-8 (−0.26 V *vs.* NHE) cannot reduce the surface absorbed O_2 to $O_2^{\bullet-}$ (−0.33 *vs.* NHE) [31]. However, due to the efficient valence band of ZnO@ZIF-8 (2.69 V *vs.* NHE), the generation of $^{\bullet}OH$ from OH^- (2.68 V *vs.* NHE) [31] is theoretically favorable. Besides, the photo-generated holes in valence band of ZnO@ZIF-8 may oxidize O_2 to produce $^1O_2$ [32]. By and large, a lower valence band edge provides holes with stronger oxidation ability, and the valence band edge of ZnO@ZIF-8 is 0.48 V lower than that of ZnO. Therefore, the higher charge-separation efficiency and stronger oxidation ability of photo-generated holes might ac-

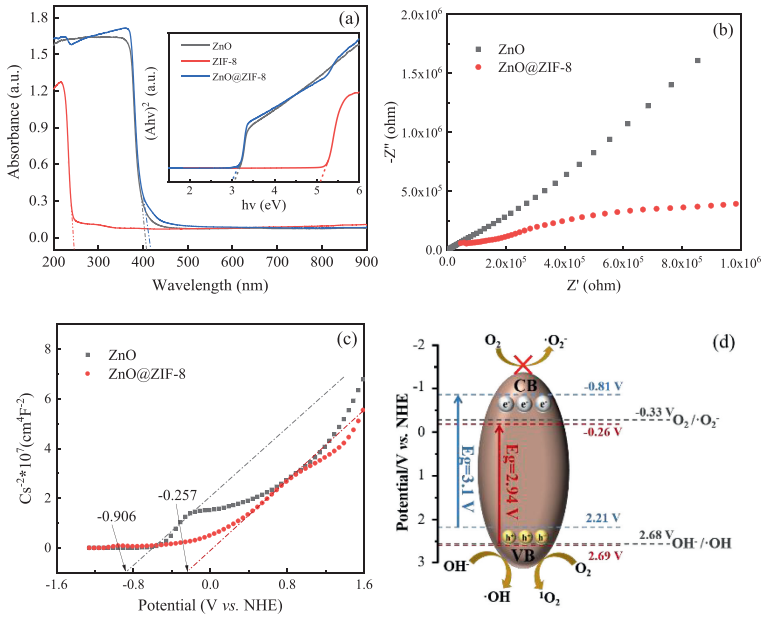

Fig. 4. (a) UV–vis DRS and Tauc curves of ZnO, ZIF-8 and ZnO@ZIF-8. (b) Nyquist plots of ZnO and ZnO@ZIF-8. (c) Mott-Schottky plots of ZnO and ZnO@ZIF-8. (d) Energy band structures of ZnO (in blue) and ZnO@ZIF-8 (in red). For interpretation of the references to color in this figure legend, the reader is referred to the web version of this article.

count for enhanced disinfection efficiency of ZnO@ZIF-8 compared with ZnO.

In order to find out the possible reactive oxygen species in the vis/PMS/ZnO@ZIF-8 system, specific inhibitors were used to trap potential reactive species. In detail, *tert*–butanol (TBA), methanol and L-histidine were employed as inhibitors for ·OH, ·OH and $SO_4^{\cdot-}$, and $^1O_2$, respectively [33-35]. First of all, *E. coli* activities in different inhibitor solutions were discussed. The control experiments showed that 10 mmol/L TBA, methanol or L-histidine barely affect the bacterial reproduction ability (Fig. S4 in Supporting information). As mentioned above, TBA is an efficient scavenger for ·OH and methanol for ·OH and $SO_4^{\cdot-}$. It can be specific that there were almost no different inhibitions on bacterial inactivation efficiency between TBA and methanol, suggesting that $SO_4^{\cdot-}$ may not work in this case. But there still was a tender inhibition of TBA and methanol on bacteria inactivation, indicating that a small quantity of ·OH existed in the system and acted on bacteria causing bacterial death. As Fig. 5a displays, the addition of L-histidine remarkably inhibited the cell inactivation efficiency, demonstrating that $^1O_2$ was the main reactive oxygen species.

To further identify the dominant ROS, EPR characterization was carried out by using 5,5-dimethyl-1-pyrroline N-oxide (DMPO) as spin trapping reagent for hydroxyl radicals and sulfate radicals [36], and 2,2,6,6-tetramethylpiperidine (TEMP) for singlet oxygen [37]. As shown in Fig. 5b, nearly no distinct signals of DMPO-$O_2^{\cdot-}$ and DMPO-·OH were observed in the system. The former phenomenon was consistent with previous discussion of ZnO@ZIF-8 photocatalytic performance. The latter might be attributed to its low content of ·OH in the system. Hence, the absence of DMPO-·OH EPR signal was confirmed by a fluorescent method with terephthalic acid as a probe [38]. We found that vis/ZnO@ZIF-8 system could produce very small amount of hydroxyl radicals, while vis/PMS and PMS/ZnO@ZIF-8 systems had a higher generation of hydroxyl radicals (Fig. 5c), suggesting PMS could generate or oxidize hydroxyl to hydroxyl radicals in aqueous solution [39]. Unsurprisingly, the fluorescent spectra intensity of vis/PMS/ZnO@ZIF-8 was the highest, exhibiting a synergy effect between photocatalysis and PMS. Meanwhile, with prolonged reaction time, the fluorescent intensity increased (Fig. 5d), revealing the system kept producing hydroxyl radicals and contributed to a better disinfection performance.

Since the reaction happened in saline solution, the detection of NaClO was conducted. As previous research reports, celestine blue (CB) could indicate the generation of NaClO. Normally, the maximum absorption wavelength of CB is around 650 nm, but would blue shift to 520 nm when NaClO exists [40]. The results elaborated that little NaClO was produced in vis/PMS/ZnO@ZIF-8 system (Fig. S5 in Supporting information), then bactericidal efficacy of NaClO is negligible. Besides, Zn^{2+} leaching in vis/PMS/ZnO@ZIF-8 system was detected and *E. coli* survival in different Zn^{2+} concentrations was studied (Fig. S6 in Supporting information), because the high concentration of Zn^{2+} is nocuous to bacteria [41]. The results verified that 2.3 mg/L leaching Zn^{2+} was avirulent to *E. coli*, the reactive oxygen species produced in the photocatalytic process were the key factors of bacterial inactivation.

The cell walls of *E. coli* are more than envelopes protecting the essential cell functions, they contain the systems of materials transport and information transfer [42]. The integrity and permeability of cell wall and membrane are basic for bacteria daily metabolism. Once gets broken, the cell would turn into inactivation. In this study, the integrity of cell membranes was investigated by laser confocal scanning microscopy (LCSM) with cell membrane fluorescent staining (Text S3 in Supporting information). As shown in Fig. 6a, with the progress of reaction, the number of damaged cell membranes increased. Till 50 min, almost all the cells died, and membranes got smashed. Additionally, SEM was employed to investigate the *E. coli* lesion process during the treatment, depicting the cell wall tattered process vividly (Fig. S7 in Supporting information). The cell morphological structure was intact at the initial stage, then the cell wall got ruptured and totally changed to fragmented, revealing the active species attacked the cell wall at first [43]. Nevertheless, the LCSM results could only qualitatively reflect a trend, but could not quantitatively analyze the results. Then flow cytometer analysis of staining bacteria was conducted. It can be seen in Fig. 6b, after a 30-min reaction, only 28.56% cell walls got broken but soon reached 98.87% at 50 min, the results present a similar trend as LCSM. Besides, it can be clearly observed that the ROS broken membranes slowly at the beginning

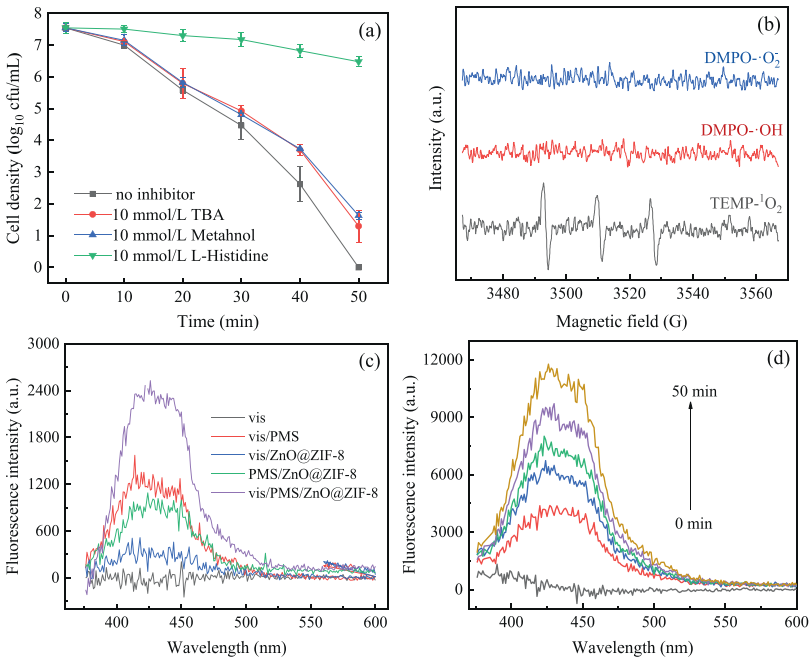

Fig. 5. (a) Bacterial inactivation efficiency in vis/PMS/ZnO@ZIF-8 system with different free radical inhibitors. (b) EPR spectra of free radicals in vis/PMS/ZnO@ZIF-8 system. (c) Fluorescence spectra of hydroxyl radicals in vis/PMS/ZnO@ZIF-8 system and control systems including vis, vis/PMS, vis/ZnO@ZIF-8 and PMS/ZnO@ZIF-8. (d) Fluorescence spectra of hydroxyl radicals in vis/PMS/ZnO@ZIF-8 system. Experimental conditions: T = 25 °C; [ZnO@ZIF-8] = 100 mg/L; [PMS] = 0.05 mmol/L; pH_0 = 6.5; $\lambda \geq 400$ nm.

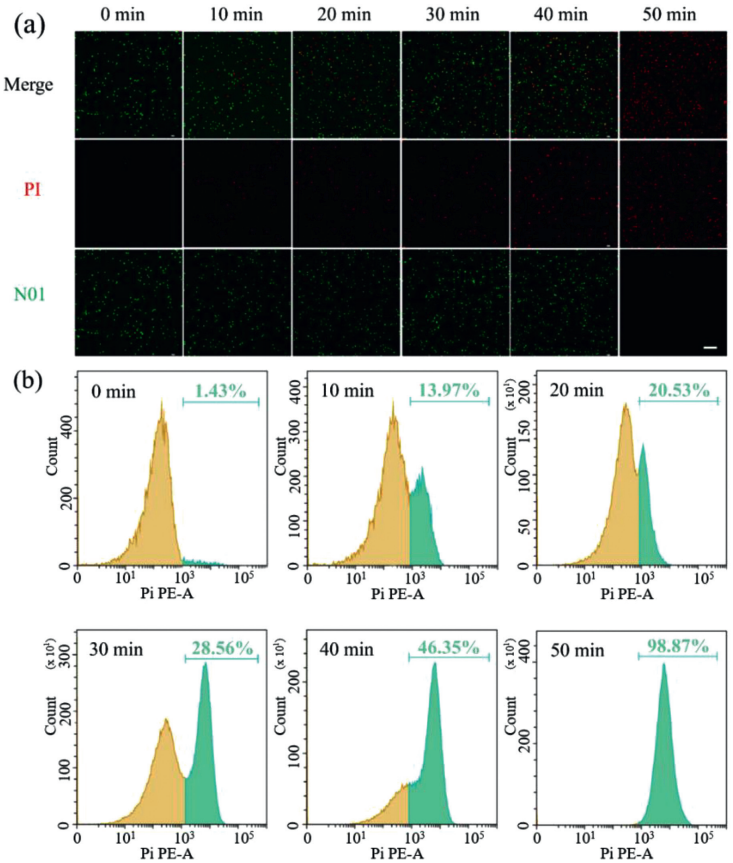

Fig. 6. Bacterial fluorescent staining in vis/PMS/ZnO@ZIF-8 system: (a) analysis of laser confocal scan microscopy, the scale bar is 10 μm. (b) Flow cytometer analysis. Experimental conditions: T = 25 °C; [ZnO@ZIF-8] = 100 mg/L; [PMS] = 0.05 mmol/L; pH_0 = 6.5; $\lambda \geq 400$ nm.

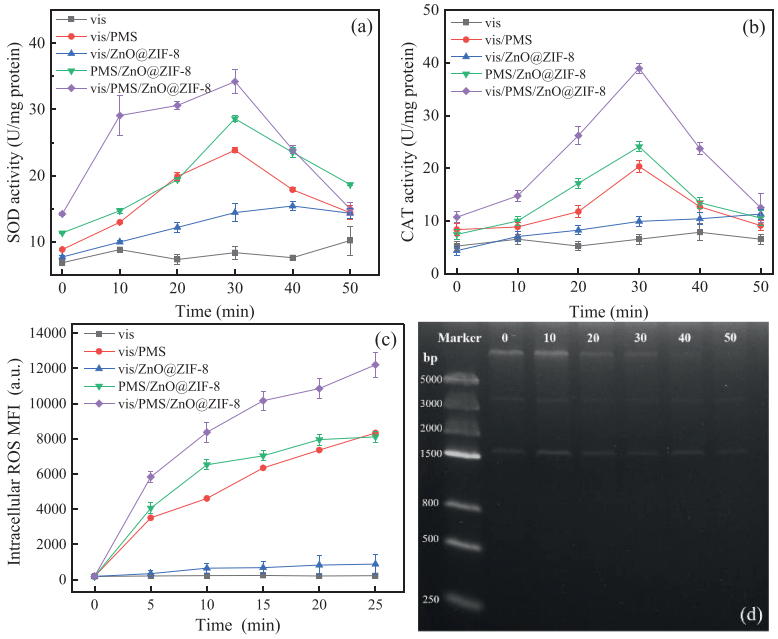

Fig. 7. (a) Bacterial SOD activity; (b) bacterial CAT activity; (c) Intracellular ROS levels of different bacteria inactivation systems; (d) DNA agarose gel electrophoresis of *E. coli* in vis/PMS/ZnO@ZIF-8 system. Experimental conditions: T = 25 °C; [ZnO@ZIF-8] = 100 mg/L; [PMS] = 0.05 mmol/L; pH_0 = 6.5; $\lambda \geq 400$ nm.

but changed to be more efficient after 30 min, which is also consistent with the results of plate count method (Fig. S8 in Supporting information). In all, it can be confirmed that cell wall was damaged in the inactivation process, which means *E. coli* lost its reproduction ability.

Moreover, to explore cell lesions mechanism caused by active species generated in vis/PMS/ZnO@ZIF-8 system, two major intracellular enzymatic activities were analyzed during the treatment process. Normally, free radicals play an important role in organisms to keep the metabolic process such as providing and transmitting energy, transcribing and expressing information. Maintaining the balance of oxidation and antioxidation *in vivo* is the basic guarantee for microbial metabolism, once broken, the oxidative stress would be induced [44]. Superoxide dismutase (SOD) and catalase (CAT) are major scavenging enzymes for cell defense against oxidative stress [45]. As Figs. 7a and b display, in vis/PMS/ZnO@ZIF-8 system, the SOD and CAT levels increased rapidly at the beginning and reached the highest value at 30 min, then gradually decreased to the thorough bacterial inactivation. It indicates that bacterial cells were encountering oxidative stress, which inducing secreting a high concentration of antioxidation enzymes to wipe out ROS. It can be speculated that the slow bacteria inactivation rate at the initial stage was attributed to the enzyme activities. However, cell apoptosis would be caused when ROSs excessively attacking the cellular defense system. Besides, compared with vis/PMS/ZnO@ZIF-8 system, the SOD and CAT levels in vis/PMS and PMS/ZnO@ZIF-8 systems were much lower, suggesting the lower oxidative stress in those systems and led to lower bacterial inactivation efficiency. Additionally, oxidative stress can up-regulate the intercellular reactive oxygen species level such as $O_2^{\bullet-}$, $^{\bullet}OH$ and H_2O_2, which would damage intercellular proteins and organelles. To further study the intercellular ROS levels, a widely-used fluorescent probe DCFH-DA was applied. In Fig. 7c, we can see the intercellular ROS kept increasing with time, and the intensity of vis/PMS/ZnO@ZIF-8 system was the highest. Then the intercellular ROS would oxidize protein, cytoplasm and even DNA (Fig. 7d), inactivating the cellular replication process through preventing DNA from unwinding and finally leading to irreparable cell injury.

Based on the above results, we propose a tentative mechanism of bacterial inactivation in vis/PMS/ZnO@ZIF-8 system in Fig. 8. Two major processes might happen in this system: (1) Photogenerated electrons on the conduction band of ZnO@ZIF-8 transfer to the adsorbed PMS and then lead to the sensitization of PMS to generate $SO_4^{\bullet-}$ (Eqs. 1 and 2), then $SO_4^{\bullet-}$ oxidize H_2O to produce $^{\bullet}OH$ (Eq. 3). The addition of PMS trapped CB electrons could promote the reduction of electron-hole recombination, which further improving the photocatalytic process. Besides, photo-generated holes on the valence band of ZnO@ZIF-8 oxidize hydroxyl and O_2 in aqueous to $^{\bullet}OH$ and $^1O_2$ (Eqs. 4 and 5). (2) The adsorbed PMS on the surface of ZnO@ZIF-8 can spontaneously dissociate to produce $^1O_2$ (Eq. 6) [46]. In detail, rich holes of ZIF-8 can assemble dispersive PMS molecules in water and provide a platform for them to generate $^1O_2$ as Eq. 6 describes. In consequence, $^1O_2$ and $^{\bullet}OH$ were the effective active species in vis/PMS/ZnO@ZIF-8 system, in which $^1O_2$ was the dominant ROS to inactivate cells.

$$\text{vis} + \text{ZnO@ZIF} - 8 \rightarrow e^-_{CB} + h^+_{VB} \quad (1)$$

$$HSO_5^- + e^-_{CB} \rightarrow SO_4^{\bullet-} + OH^- \quad (2)$$

$$SO_4^{\bullet-} + H_2O \rightarrow {}^{\bullet}OH + SO_4^{2-} + H^+ \quad (3)$$

$$OH^- + h^+_{VB} \rightarrow {}^{\bullet}OH \quad (4)$$

$$O_2 + h^+_{VB} \rightarrow {}^1O_2 \quad (5)$$

$$HSO_5^- + SO_5^{2-} \rightarrow SO_4^{2-} + HSO_4^- + {}^1O_2 \quad (6)$$

In practical applications, the reusability and regeneration of photocatalyst are of vital importance. In order to investigate the reusability, used ZnO@ZIF-8 was collected by centrifugation and washed in deionized water with 2-h ultrasound, then dried in a thermostatic drying oven for reuse. The treated effluent was discarded, and fresh bacterial suspension of 7.5-log cfu/mL would be disposed with recycled catalyst. As the results are shown in Fig.

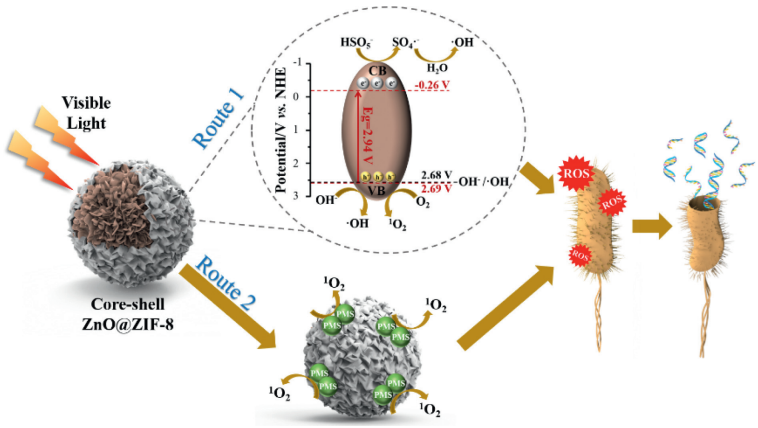

Fig. 8. Schematic illustration of bacterial inactivation mechanism in vis/PMS/ZnOZIF-8 system.

S9 (Supporting information), in the previous three runs, almost all of the bacteria could be inactivated in 50 min with the treatment of vis/PMS/ZnOZIF-8, demonstrating a stable bactericidal efficiency. Nonetheless, the inactivation efficiency fell to 67.32% and 61.3% from 99.99% in the fourth and fifth run, respectively. The composition and structure of the used catalyst were analyzed by FT-IR and XRD to search for a reason for those phenomena. The consequences elaborated a significant reduction of ZIF-8 shell (Fig. S10 in Supporting information), which might due to photo-corrosion on the surface of ZnO@ZIF-8 [47]. Hence, it is necessary to further modify the photocatalyst to reduce photo-corrosion effect and improve the reusability in practical applications. As previous studies report, a polyaniline coat or a graphene shelter would be helpful to enhance photo-corrosion resistance during the photocatalysis process [48,49], which might be good means to modify ZnO@ZIF-8.

In this work, a core-shell ZnO@ZIF-8 was synthesized and applied for bacteria inactivation under visible light. We found that the ZIF-8 shell was uniformly covered on the surface of ZnO core. The ZIF-8 shell significantly enhanced photocatalytic bacteria inactivation efficiency than pure ZnO microspheres and provided an excellent surface for adsorbing dissociative PMS in aqueous. Besides, it only took 50 min to achieve thorough bacteria inactivation for 7.5-log cfu/mL and 30 min for 6.5-log cfu/mL, demonstrating an efficient disinfection performance. The vis/PMS/ZnO@ZIF-8 system remained excellent disinfection efficiency in different pH (3, 5, 7 and 9). The mechanism of enhanced photocatalytic performance was analyzed by UV–vis DRS and photoelectrochemical methods including EIS spectra and Mott-Schottky plots. The improved photocatalytic efficiency was attributed to the core-shell structure of ZnO@ZIF-8, which led to a better charge-separation efficiency and stronger oxidation ability of photo-generated holes. Then ROS in the system were studied by free radical quenching experiments, EPR characterization and fluorescent method, demonstrating $^{\bullet}OH$ and $^{1}O_2$ were the active species in the system and the latter played the leading role. Furthermore, the bactericidal mechanism was analyzed by the integration of cell wall, enzyme activity, intercellular ROS and genome size. We found that the active species in the system attacked the cell wall first, broke the balance between cellular oxidation and antioxidation, then induced up-regulation of intercellular ROS to disintegrate cell and DNA. These results were expected to provide advanced information about water disinfection and the visible light photocatalytic process.

Declaration of competing interest

The authors declare that they have no known competing financial interests or personal relationships that could have appeared to influence the work reported in this paper.

Acknowledgments

The authors would like to acknowledge the financial support from National Natural Science Foundation of China (No. 52070133), Sichuan Science and Technology Program: Key Research and Development Program (Nos. 2019YFG0314, 2017SZ0180, 2019YFG0324). The authors would like to thank the Analytical & Testing Center of Sichuan University for EPR detection.

Supplementary materials

Supplementary material associated with this article can be found, in the online version, at doi:10.1016/j.cclet.2021.06.058.

References

[1] UNICEF, W.H.O., Progress on household drinking water, sanitation and hygiene 2000-2017: Special focus on inequalities, New York, 2019.
[2] P. Moffitt, W. Aujla, C.J. Giesbrecht, I. Grant, A.L. Straatman, J. Family Violence (2020), doi:10.1007/s10896-020-00212-x.
[3] D. Ghernaout, N. Elboughdiri, S. Al Arni, J. Water Reuse Desal. 10 (2020) 173–186.
[4] H. Wang, C. Hu, X. Hu, Eng. Fail. Anal. 39 (2014) 12–20.
[5] D.E. John, C.N. Haas, N. Nwachuku, C.P. Gerba, Water Res. 39 (2005) 2369–2375.
[6] S. Delacroix, C. Vogelsang, A. Tobiesen, H. Liltved, Mar. Pollut. Bull. 73 (2013) 24–36.
[7] T.A. Alkanhal, I. Tlili, J. Water Reuse Desal. 9 (2019) 232–248.
[8] S. Percival, R. Chalmers, M. Embrey, et al., Microbiology of Waterborne Diseases, Academic Press, London, 2004.
[9] J. Li, Y. Li, Z. Xiong, G. Yao, B. Lai, Chin. Chem. Lett. 30 (2019) 2139–2146.
[10] T.P. Yoon, M.A. Ischay, J. Du, Nat. Chem. 2 (2010) 527–532.
[11] M.C. Uribe-López, M.C. Hidalgo-López, R. López-González, et al., Photochem. Photobiol. 404 (2021) 112866.
[12] S.G. Ullattil, M.J.J. Fatima, A. Abdel-Wahab, Environ. Sci. Poll. Res. 27 (2020) 37036–37043.
[13] J. Podporska-Carroll, A. Myles, B. Quilty, et al., J. Hazard. Mater. 59 (2015) 669–678.
[14] H.L. Jiang, B. Liu, T. Akita, et al., J. Am. Chem. Soc. 131 (2009) 11302–11303.
[15] S. Nimai, H. Zhang, Z. Wu, N. Li, B. Lai, Chin. Chem. Lett. 31 (2020) 2657–2660.
[16] X. Wang, X. Pu, Y. Yuan, et al., Chin. Chem. Lett. 31 (2020) 2634–2640.
[17] W. Wang, H. Wang, G. Li, et al., Water Res. 157 (2019) 106–118.
[18] M.C. Uribe-López, M.C. Hidalgo-López, R. López-González, et al., J. Photochem. Photobiol. A 404 (2021) 112866.

[19] B. Yu, F. Wang, W. Dong, et al., Mater. Lett. 156 (2015) 50–53.
[20] S.İ. Dönmez, S.H. Needs, H.M.I. Osborn, A.D. Edwards, Sens. Actuator. B 323 (2020) 128645.
[21] G. Ren, Z. Li, W. Yang, et al., Sens. Actuator. B 284 (2019) 421–427.
[22] H. Jiang, Q. Yan, Y. Du, R. Chen, React. Kinet., Mech. Catal. 117 (2016) 307–317.
[23] K. Subramani, M. Sathish, Mater. Lett. 236 (2019) 424–427.
[24] J. Moreno-Andrés, J. Morillo-Ponce, M.E. Ibáñez-López, A. Acevedo-Merino, J.L. García-Morales, J. Environ. Chem. Eng. 8 (2020) 104335.
[25] M. Karbasi, F. Karimzadeh, K. Raeissi, S. Giannakis, C. Pulgarin, Chem. Eng. J. 396 (2020) 125189.
[26] C. Qi, X. Liu, J. Ma, et al., Chemosphere 151 (2016) 280–288.
[27] W. Wang, H. Wang, G. Li, P.K. Wong, T. An, Water Res. 176 (2020) 115746.
[28] Z. Chen, N. Zhang, Y.J. Xu, Cryst. Eng. Comm. 15 (2013) 3022–3030.
[29] G. Huang, R. Shi, Y. Zhu, J. Mol. Catal. A 348 (2011) 100–105.
[30] Y. Liang, T. Novet, J.E. Thorne, B.A. Parkinson, Phys. Status Solidi A 211 (2014) 1954–1959.
[31] P. Wardman, J. Phys. Chem. Ref. Data 18 (1989) 1637–1755.
[32] Q.Y. Yu, G.Y. Zhai, T.L. Cui, et al., Sci. China 62 (2019) 434–439.
[33] L. Kong, M. He, Environ. Sci. Technol. 50 (2016) 6974–6982.
[34] M.K. Sahoo, L. Sayoo, D.B. Naik, R.N. Sharan, Sep. Purif. Technol. 106 (2013) 110–116.
[35] T.A. Dahl, W.R. Midden, P.E. Hartman, Photochem. Photobiol. 47 (1988) 357–362.
[36] M.J. Davies, Methods 109 (2016) 21–30.
[37] K.C. Das, C.K. Das, Biochem. Bioph. Res. Comm. 295 (2002) 62–66.
[38] K.-i. Ishibashi, A. Fujishima, T. Watanabe, K. Hashimoto, Electrochem. Commun. 2 (2000) 207–210.
[39] M. Ahmadi, F. Ghanbari, M. Moradi, Water Sci. Technol. 72 (2015) 2095–2102.
[40] I.S. Donskyi, O. logo, Y. Chen, et al., Nanoscale (2020) 14222–14229.
[41] M.B. Spesia, M. Rovera, E.N. Durantini, Eur. J. Med. Chem. 45 (2010) 2198–2205.
[42] V. Braun, K. Rehn, Eur. J. Biochem. 10 (1969) 426–438.
[43] Y. Chen, X. Tang, X. Gao, et al., Ceram. Int. 45 (2019) 15505–15513.
[44] J.H. Kim, E.Y. Park, H.K. Ha, et al., Asian Austral. J. Anim. 29 (2016) 288–298.
[45] R. Mittler, Trends Plant Sci. 7 (2002) 405–410.
[46] X. Mi, P. Wang, S. Xu, et al., Angew. Chem. Int. Ed. 60 (2020) 4588–4593.
[47] X. Ma, H. Li, T. Liu, et al., Appl. Catal. B 201 (2017) 348–358.
[48] H. Kim, B.L. Yang, New J. Chem. 43 (2019) 16699–16705.
[49] M. Wang, L. Cai, Y. Wang, et al., J. Am. Chem. Soc. 139 (2017) 4144–4151.